July 2016

Designing Active Granular Squares

Christopher C. Olson
University of Massachusetts Amherst

DESIGNING ACTIVE GRANULAR SQUARES

A Thesis Presented

by

CHRISTOPHER OLSON

Submitted to the Graduate School of the
University of Massachusetts Amherst in partial fulfillment
of the requirements for the degree of

MASTER OF SCIENCE

May 2016

Physics

DESIGNING ACTIVE GRANULAR SQUARES

A Thesis Presented

by

CHRISTOPHER OLSON

Approved as to style and content by:

Narayanan Menon, Chair

Don Candela, Member

Rory Miskimen, Department Head
Physics

ACKNOWLEDGMENTS

Thanks to Lee Walsh for all his patience, and his help. Thanks to Sarah Schlossberg for all her efforts towards designing active squares.

ABSTRACT

DESIGNING ACTIVE GRANULAR SQUARES

MAY 2016

CHRISTOPHER OLSON

B.Sc., LEWIS AND CLARK COLLEGE

M.S., UNIVERSITY OF MASSACHUSETTS AMHERST

Directed by: Professor Narayanan Menon

The goal of this thesis has been to find a means of i) designing an active square particle, and ii) continuously varying its degree of activity with the objective of understanding the effects of activity on the various phases of granular matter. The motivations, results and limitations of our methods of creating active particles are discussed in this thesis. The applicability of the stochastic model based on the Langevin equation in 2D as well as implications for future experiments are also discussed.

TABLE OF CONTENTS

LIST OF FIGURES

INTRODUCTION

Active matter consists of large aggregations of self propelled particles or agents. The most general requirement is that each member of the aggregate have some intrinsic directed motion, or internal drive, fueled by local energy consumption. Energy is explicitly not conserved and often particle number and momentum are not conserved either. The group as a whole then, remains out of thermodynamic equilibrium. Unlike many other non-equilibrium systems energy consumption happens homogeneously throughout the system instead of at the boundaries [1], and no external field or force controls the alignment or motion of the particles. As a result new non-equilibrium statistical methods are required in the modeling of such systems.

Most examples of active matter are biological in nature: from microtubules and actin motors, to bacterial colonies, swarms of insects and fish, flocks of birds or large groups of land mammals including humans[1-7]. There are however a number of synthetic examples, from dry granular systems to active colloidal suspensions, and swarm robotics [1,2,8-16]. In modeling active systems the individuals are assumed to move and interact through a set of usually simple rules, for instance aligning one's velocity vector with the average velocity inside some neighborhood. The interactions, though simple, can nonetheless result in a number of interesting emergent properties and the display of novel phenomena including: flocking/swarming, collective motion and alignment in the absence of centralized control, and giant number fluctuations. Further phenomena seen in a number of equilibrium systems are also observed including: spontaneous symmetry breaking, nematic order, phase separation, clustering, long-range order.

As this list might suggest, much of the literature of phase transitions has been brought to bear on the issue, and the phases of various active systems is a subject of much study. Indeed, the image of interacting spins, or axisymmetric bodies readily invites comparisons to various Ising models with the critical distinction that the individual elements are not fixed within a lattice. [2,5-7,17-19]. The abundance of this unique form of condensed matter further impels the physics community to study the associated problems. Most existing theory on the subject currently makes use of either a stochastic approach based on the Langevin equation or one of coarse-grained hydrodynamic field theories.

Our lab is interested in issues concerning active granular physics. Large aggregations of mammals, birds or fish, are difficult to control, as well as measure [3]. More small scale biological experiments often require external chemical gradients which can exert a strong influence and are hard to evaluate[2,14]. Furthermore there is the problem of flow in the surrounding media of active gels or colloids. The interplay between activity, local alignment, and the medium is at best complicated [1,2].

Granular matter has no long-range interactions. Such systems have the advantage of being conceptually and experimentally very clean, or simple to realize. As a result they have the potential to be very controlled, minimal, model experiments. Many are macroscopic in scale (ranging from hundreds of microns in size up to centimeters), and use comparatively simple detection schemes. The size scale of such experiments enables the use of standard digital imaging devices, which are all the more streamlined and easy to implement due to their ubiquitous use for more commercial reasons. Experimental realizations involve large numbers of particles that can be created lithographically, micro-machined, 3D printed, or purchased in bulk relatively cheaply. Often such systems are modeled or realized as 2D monolayers of fluidized grains, beads, or rods. Much preliminary work has been done with either

disk-like or rod-like shapes in 2D, and a great deal of the above phenomena have been observed in these simple granular systems[8-10,14,16].

That different active systems display similar phenomena on a multiplicity of scales and conditions suggests that the dynamics governing their collective behavior are universal. Here we focus on fundamental symmetry properties as being responsible for some of their more outstanding features [2,5-7,17-19]. Any property of a system (observable or intrinsic) that remains unchanged after some transformation or action falls into the category of a physical symmetry. The loss of such a property is called 'symmetry breaking'. Quite often disparate systems which belong to the same symmetry group will behave in the same way under a given transformation or action. The effect of locating a symmetry in your system is to reduce a portion of your problem to one that has already been solved. Such properties have immense explanatory power and have played a large role in the study of phases in equilibrium systems. Attempting to account for the numerous different interactions of a system and its environment can significantly complicate any model, and may often be unnecessary.

Within the context of my experiment special attention is paid to two different kinds of symmetries. First there is the polar motion of the particle, where a single vectorial direction of motion is picked out. Second is the square symmetry with respect to the particle's interactions with its neighbors. Because each particle is square, any rotation by an integer multiple of $\frac{\pi}{2}$ leaves the steric interaction with its neighbors unchanged. Symmetry considerations, both in interaction and motion are key in attempting to find minimal models that capture all the features of the observed phenomena. For example it has been shown that collective motion, polar order, and giant number fluctuations can occur for active disks (in 2D) despite their rotationally symmetric *interactions*. Polar symmetry with respect to particle *motion* is one of the fundamental ingredients needed in order for such a thing to occur (the other is lack of momentum conservation)[14]. No innate sensing capability, or complicated

alignment interactions need be posited. Those systems that move both backwards and forward along their body axis (i.e. nematic symmetry of motion) do not display the same phenomena. They belong to different symmetry groups [2,5-10,14,16-19]. Despite their simplicity (in fact because of it) granular experiments may yet have implications for understanding or effecting a diversity of other systems.

CHAPTER 1

THE EXPERIMENT

The subject of the experiment is active square particles. We would like to look at the effects of a four-fold interaction symmetry, and polar activity on the phases of active granular matter. The need for a particle with a directed motion persistent enough, while still satisfying the various shape requirements became the object of my efforts. In order to truly characterize the system as 'active', the constituents need to display persistent motion. The desired motion in this case would simply be forward along one horizontal body axis. At the limit of having no internal velocity or preferred axis of motion the system appears as one of brownian squares, their motion entirely diffusive.

Our experiment consists of a collection of fluidized macroscopic square particles enclosed in a flat horizontal cell, driven by an electromagnetic shaker. Squares occupy an unexplored middle ground between elongated nematics or rods, and rotationally symmetric discs. Another motivation for the choice of square particles is the subtlety found in the phase diagrams for convex polygons due to the competition between tendencies to maximize translational and rotational entropy [20-23]. Furthermore there has been a general lack of experiments involving particles whose interactions and activity lack the same symmetry (those of Deseigne *et al.* being an obvious exception). Exploring this option should go a long way towards determining those aspects of the system's phases that are truly due to activity, and not just shape entropy.

As squares they possess a discrete interaction symmetry with respect to their neighboring particles. Each particle also has a built-in vertical *a*symmetry (discussed below). This results in a preferred axis, internal to the particle itself, along which it tends to move. This asymmetry is polar, and thus the particle tends to move in a single direction relative to this axis. In addition, the particles' dynamics in the dilute limit also show long-time brownian or diffusive motion (despite their polar activity, and shape) resulting from random collisions with each other and the environment. The particles interact through excluded volume. The vibration of the cell constitutes an energy source; inelastic collisions with the floor, lid, and other particles lead to a steady state.

1.1 Model

In describing the phases of our active system it is useful to look at the behavior of a number of its correlation functions and order parameters. Of most immediate interest in this experiment were the mean squared displacement, position-orientation cross correlation, and the orientation autocorrelation. These can be derived from a set of stochastic differential equations based on the Langevin Equation in 2D [24,25]. The existing model was produced by collaborator Aparna Baskaran of Brandeis University. The two dimensional motion of a particle with some intrinsic velocity in such a heat bath can be described as follows:

$$m(\frac{d\vec{v}(t)}{dt}) = -m\gamma\,\vec{v}(t) + \vec{\eta}(t) + m\zeta\,\vec{v}_0, \tag{1}$$

$$\frac{d\theta}{dt} = \xi(t) \tag{2}$$

The first term on the right hand side of equation (1) is a damping associated with an increased rate of particle collisions, and thus drag, when a particle achieves higher velocities. The second term constitutes a sort of noise imparted to the particle through

collisions with its neighbors. The final term is a constant velocity possessed by the particle. Equation (2) describes the angular velocity of the particle with respect to a global x-y axis that remains fixed in time. This term is purely noise. Here both $\vec{\eta}(t)$ and $\xi(t)$ are gaussian random variables. Each is assumed to be delta correlated in time, i.e. $< \vec{\eta}(t)\,\vec{\eta}(t') >= 2D_T\delta(t-t')$, and $< \xi(t)\,\xi(t') >= 2\,D_R\delta(t-t')$, where D_T and D_R are the coefficients of translational and rotational diffusion.

Our system operates in the overdamped limit. The particles cease their motion almost the instant our external energy source is turned off. In this limit γ is quite large, meanwhile $\vec{\eta}(t)$ and ζ, which are both fundamentally related to γ are likewise large [24-26]. The simplified equations (after re-scaling to temporarily eliminate tedious constants) appear as:

$$\vec{v}(t) = \vec{v}_0 + \vec{\eta}(t), \tag{3}$$

and

$$\frac{d\theta}{dt} = \xi(t), \tag{4}$$

The above are somewhat further simplified in that they only represent a single dimension, when in fact our system is two dimensional. The orientation vector appears as:

$$\vec{n}(t) = \hat{n}\,e^{i\,\theta(t)}, \qquad n_x = \cos\left(\theta(t)\right), \quad and \quad n_y = \sin\left(\theta(t)\right) \tag{5}$$

The velocity is generally understood to be taken along the direction of the orientation vector, though at any given time we usually only speak of one component as x and y remain independent of one another. From these two equations a number of useful things can be derived. As mentioned, the quantities most relevant to my

experiment are the mean squared displacement ($< \vec{r}(t)\,\vec{r}(t+t_0) >$), the orientation autocorrelation ($< \vec{n}(t)\,\vec{n}(t+t_0) >$), and the position-orientation cross correlation ($< \vec{r}(t)\,\vec{n}(t+t_0) >$). Given equations (3) and (5), these can be worked out and appear as follows [26]

$$< \vec{r}(t)\,\vec{r}(t+t_0) >= 2(\frac{v_0}{D_R})^2\,(D_R\,t + e^{-D_R\,t} - 1) + 2\,D_T\,t \tag{6}$$

$$< \vec{n}(t)\,\vec{n}(t+t_0) >= (\frac{1}{2})\,e^{-D_R\,t} \tag{7}$$

$$< \vec{r}(t)\,\vec{n}(t+t_0) >= (v_0/2D_R)\,(1 - e^{-D_R\,|t|})sign(t) \tag{8}$$

The quantity ($\frac{v_0}{D_R}$) gives a measure of the particle's persistence length (in units of particle length) and became a metric of primary concern in deciding what constituted a 'good' particle design. D_R is the inverse decay time for a particle's orientation measured in the natural units of our system where one time-step corresponds to one period of oscillation of the shaker. By measuring the above correlation functions in our data we can compare the shape of the resulting plots with those predicted by the model. The free parameters in fitting correspond to v_0, D_T, and D_R for our particles. From these we can learn about the locomotion executed by the particles, and get a sense of their persistence length ($\frac{v_0}{D_R}$). Having a sufficiently large persistence length is necessary in order to define our particles as being active at all. If, through rotational noise, our particles forgot their direction of motion within a very short time, their dynamics would appear much more brownian. The phenomena we hope to investigate depend on their being active particles. Having a persistence length of one particle body length per rotational diffusion time (D_R^{-1}) served as a rough dividing line between 'active' and 'inactive' through the course of the experiment.

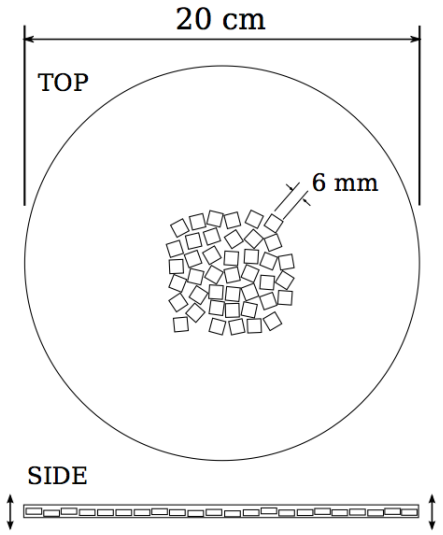

Figure 1.1: Top down and profile illustration of the plate/particle chamber.

1.2 The Setup

The experimental setup detailed below was designed and implemented by fellow lab member Lee Walsh. The particles exist in a monolayer between two horizontal plates, separated by a vertical spacer. The lower plate is made from aluminum (20 cm. diameter), the upper is clear acrylic. The spacer height varied between 4.75 and 6.35 mm, and the particles at rest had a gap between them and the lid varying from .127-1.27 mm (Fig. 1.1).

The chamber is attached to a rigid square column that runs through a forced air collar to stabilize the vibration and minimize any non-vertical motion (Fig 1.2a). This air column is itself attached to a thinner cylindrical brass rod (with a stiff vertical, but soft horizontal and rotational coupling) bolted to an electromagnetic (LDS V455) shaker. The shaker is attached to a ballasted framework, which rests on top of a thick rubber mat to provide stabilization and insulation from outside noise (Fig 1.2b). The levelness of the plate is further ensured by tapped holes at the base of the framework, and set screws allowing for the adjustment of the tilt. The shaker is driven by an (LDS PA1000L) amplifier, whose input comes from a function generator (Hewlett

Packard 33120A Function/Arbitrary Waveform Generator) outputting a sine wave. The shaker is capable of an acceleration $\Gamma \leq 117g$ in a frequency range of 5 to 7500 Hz. Here $\Gamma = A(2\pi f)^2/g$, where g is the acceleration of gravity, A, the shaker amplitude, and f, the driving frequency. Data was taken at frequencies ranging from 50 to 100Hz. The driving frequency and gain are chosen so that the acceleration of the plate is larger than that due to gravity. In these experiments the particles were driven with an acceleration ranging from 3-12g. The vibrating chamber is imaged from above through a vertically oriented high speed digital camera (Vision Research Phantom v7.1) placed directly over the plate.

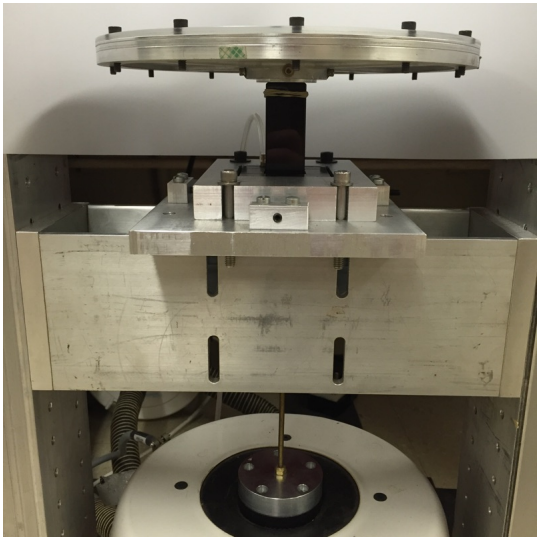

(a) Visible here is the square driving column, and its air-bearing collar.

(b) View of the base of the shaker. One can see the brass rod that leads up to the air bearing.

Figure 1.2

The particles were designed in solidworks (student edition 2015) then printed out of ABS -P430 through the department's 3D printer (uPrint SE plus, Catalyst EX). The particles are approximately 6mm in length and each is printed with a tapered leading edge so that it rests at a slight incline (Fig. 1.3a, b). The particle design shown in Fig. 1.3 was one of several.

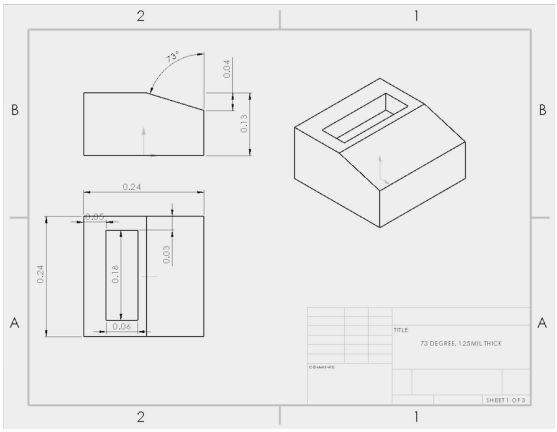

(a)

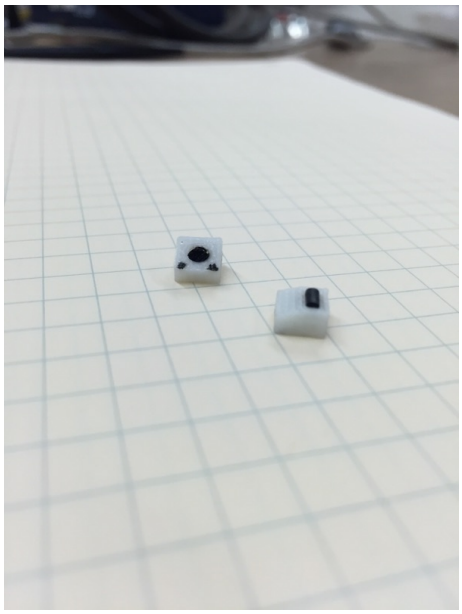

(b)

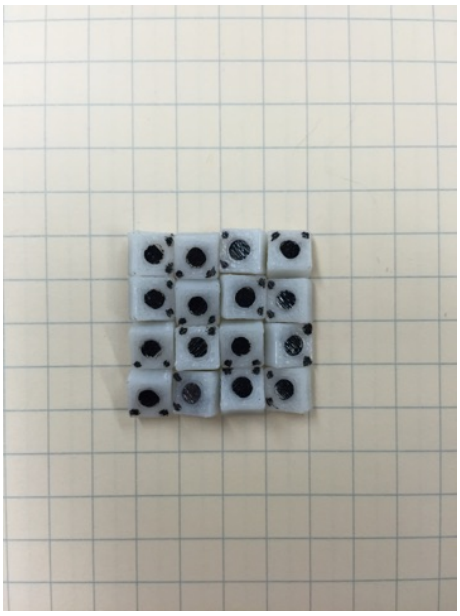

(c)

Figure 1.3: (a) Diagram of a typical particle as seen from the underside. The diagram shows the particle before the insertion of the neoprene 'foot'. (b) View of two particles, one belly up to show its rubber foot. (c) A set of particles roughly tiling a square lattice. Despite their incline, the 2D projection of the particle remains square.

In each design the tilt is kept such that the square interaction symmetry is still preserved (Fig. 1.3c). Too great an incline and the aspect ratio of the 2D particle

projection becomes skewed as they rock forward. There is also a greater chance of particle overlap with a steeper bevel. The angle of taper was one of a handful of parameters I varied in this experiment. The angle in degrees is included in the particle name. This angle is measured between a plane containing the front facet or 'nose' of the particle, and the beveled face (Fig 1.3a upper left corner).

Each design iteration is also printed with one to two shallow rectangular troughs on the upper and/or lower facet, placed toward the thicker rear end of the piece. The particle shown in Figure 1.3 has only one trough on its underside. A short length of neoprene o-ring stock of circular cross section is cut and inserted into the trough so that it just protrudes.

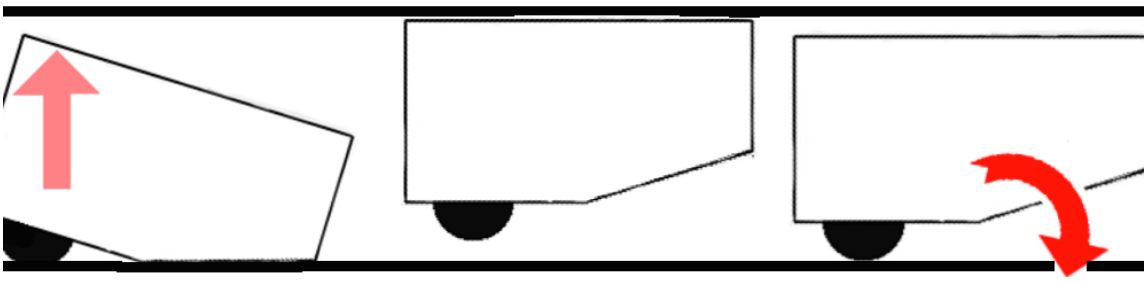

Figure 1.4: The motion of a particle of the type depicted in Figure 1.3. The particle is thrown upward by the acceleration of the shaker. It contacts the ceiling and rotates until its upper facet is parallel with the horizontal. This has the effect of moving the foot forward in space by a small amount. The particle is then accelerated downward and as it contacts the floor it both rotates until it contacts the ground.

This 'foot' (as it will be referred to from here on) has a higher coefficient of friction, and when vertically vibrated this thicker, tackier, and springy-er end of the particle results in its directed motion. A substantial fraction of the time the particle lands at a tilt relative to the horizontal. When it lands foot-first the frictional force pushes the particle forward. The asymmetry in thickness results in the rear end interacting with the plate and lid more frequently. ABS being relatively slippery when compared with neoprene, the opposite sort of push from the nose is usually much smaller, and less frequent. Thus vertical motion is converted into motion in the X-Y plane (both

translation and rotation), owing to the asymmetric shape, mass distribution, and friction of the particles.

1.3 Imaging and Detection

The particles are imaged from above with a high speed video camera. The main axis of the camera is parallel to the normal of the plate. The particles have been marked with ink dots of a color that contrasts with the ABS from which they've been printed. A tiny circular depression is printed into the upper facet of the particle which allows it to be marked by hand in a consistent manner. The large dots in their center are used to find their positions. The smaller dots near the 'nose' are used to assign the particle an orientation. The shaker and particles are lit from above, at an oblique angle, with halogen lamps (Figs. 1.5 (a), (b)).

(a)

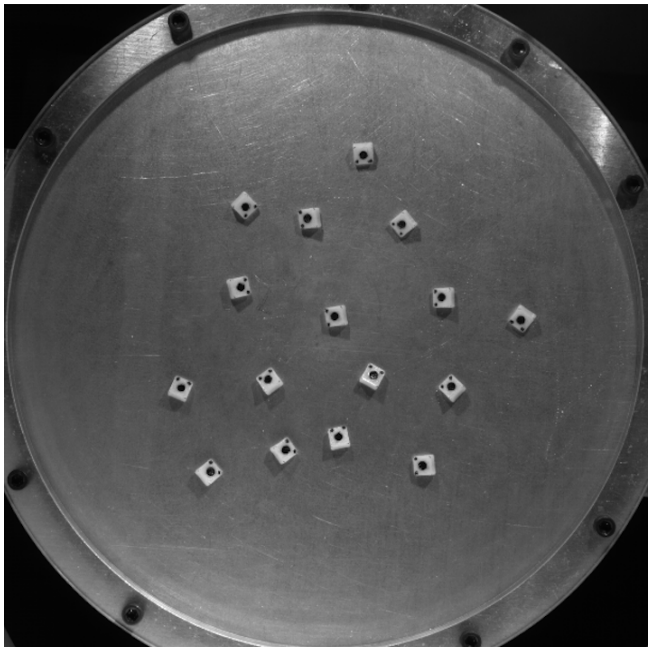

(b)

Figure 1.5: (a) A typical lighting configuration. Oblique light is cast onto the diffusing backboard (the white half cylindrical shell), thus illuminating the plate/particle chamber. (b) An example image from a typical data set. All image processing routines are run on images such as this one.

In the interest of high temporal resolution the videos are taken at 120fps with an exposure time of 400 microseconds. The aperture is set to f/8, and the image size 608x600 pixels. In addition to temporal resolution the 120 fps imaging rate was selected in order to eliminate any unwanted phasing with the fluorescent lights present in the lab, which flicker at approximately 60Hz. A non-integer multiple of this frequency would result in uneven exposure levels throughout the duration of the video, thereby making detection harder. The relevant time scales for the physics we expect to test are much longer than 1/120 of a second. The vast majority of experimental runs were done with a vibration frequency of 50Hz, giving us 2.4 frames per oscillation. The downside to increased shutter speed is a darker image, and to compensate we use halogen lamps. A matte white back-board is also used to diffuse much of this light and eliminate unwanted glare.

A given run will usually last about one minute, yielding a video of approximately 7,000 frames, to be converted to .tif files for processing later on. After converting the videos a number of image processing routines are run on the collection of tiffs in order to extract statistical information about the motion of the particles. The tracking software was developed in Python by Lee Walsh and is available online[1]. Thanks to the tracking dots, and through the use of convolution, thresholding, and segmentation algorithms we're able to find 80-90 percent of the particle locations and orientations in a given image. Because of the high frame rate a particle's trajectory may be established by iteratively stepping through each frame and locating the particle nearest its coordinates from the previous frame. After recursively checking all other particles in the same manner and attempting to resolve any conflicts in particle trajectory, a unique track or path may be assigned to a particle after stitching together its long list of coordinates from each frame. The evolution of a particle's orientation is found in

[1]https://github.com/leewalsh/square-tracking

much the same manner. In the event that a particle or orientation goes undetected in certain frames an attempt to interpolate between frames is made up to a user defined limit. For a single lost frame interpolating between points is usually uncontroversial. The history of the particle becomes much more uncertain however after say, ten dropped frames. By default if a particle's position is lost or should go undetected for more than ten frames the track is 'severed', and any reappearance of the particle is counted as the beginning of a new track. A track is also severed if the particle contacts the chamber wall, as these collisions tend to skew the statistics. From the long list of positions and times, velocities can then be established.

All of the raw data (positions, orientations, velocities), saved in a multidimensional array is then ready for analysis. The various correlation functions ($< \vec{r}(t+t_0)\vec{r}(t_0) >$, $< \vec{r}(t+t_0)\vec{n}(t_0) >$, $< \vec{n}(t+t_0)\vec{n}(t_0) >$, averaged over t_0 or frame, as well as particle) are used in determining the statistical properties of each particle set. It is also possible to examine the spatial, and temporal distribution of our rotational and translational noise, as well as a number of different order parameters, though these are not addressed here.

CHAPTER 2

RESULTS/ANALYSIS

Early attempts at designing a sufficiently active particle were carried out by Sarah Schlossberg[1] (UC San Deigo). Initial particle designs were optimized largely by the criterion of large persistence length. My first task in joining the lab was to carry on experiments, using existing particle sets, regarding the nature of active crystal melting. Some preliminary work on this had already been carried out by Michael Mueller[2]. There were still several problems at that time however, the particles weren't active enough, and they occasionally overlapped. There was also suspicion that the initial shaker oscillations in each experimental run, as the system ramped up to operating conditions, could be strongly affecting particle locomotion. These would become the core issues of my work.

The need to more carefully control the square shape of the particle became apparent after my first few experimental runs looking at melting. The asymmetry in particle shape, its tapered front edge, and the degree or incline of this asymmetry influences its persistence length. The only set considered nearly 'active enough' up until that time was printed at such a tilt to the horizontal that the possibility of nested particles, edging under one another became a real problem at high densities and during collisions. The hard-core, square potential became softer on certain sides. The first step was to make them thicker. This process contained a serious stumbling block (detailed below), but a satisfactory design was eventually achieved. When the

[1]B-SMaRT REU participant during the summers of 2014 and 2015

[2]UMass 2014-15

change in particle height yielded an unexpected increase in persistence length interest in designing a more active particle was renewed. In addition, an examination of the system start-up and the possibility of resonant modes, as well as a closer look at the specific means of particle locomotion were carried out. Up until this time the system reached its operating conditions only gradually as the gain on the driving signal was increased manually. The effects of such a finite start-up time were hard to account for and increasing the gain by hand was too uncontrolled. Further, initial experimental runs starting with a condensed lattice of particles showed an anomalous increase in mean squared displacement at early times. This prompted an look into possible resonant modes as well as the specifics of particle locomotion.

2.1 Particle Design

There are limits to the types of particles that can be 3D printed. The additive manufacturing process involves depositing many layers of ABS material to build up the final shape of the printed piece. These layers, though very small, are necessarily finite (10 mil) and this factors into how the printing software attempts to render any 3D model it receives. In attempting to render and read the STL files exported from Solidworks the Catalyst EX software can create minor defects in the layers or dimensions of the printed piece. This would become a problem in working through different particle designs. It was suggested that designing the particles with a height that measured an integer number of layers might resolve the issue but this was not the case. Tiny differences in particle design (e.g. the thickness, the placement of the trough) could result in defects appearing or disappearing. These defects are not random, but not well understood yet (Fig. 2.1 (a), (b)). The result is always an excess of printed material, but the material is not added uniformly. It usually appears as a small excess added to the underside, near one of the corners. Other times as a projection from a single side facet. Particles such as ours depend on

features on the order of the size of these defects for their locomotion. These added asymmetries have the potential to affect the motion and interaction of the particle. Their presence prevents a careful control of the activity. Given the space constraints of the shaker cell and the need to prevent particle overlap, a limited range of particle heights were considered. Of those considered, only a few were printable. A small array of alternative designs and the statistical properties associated with the motion of each can be found in section 2.3.

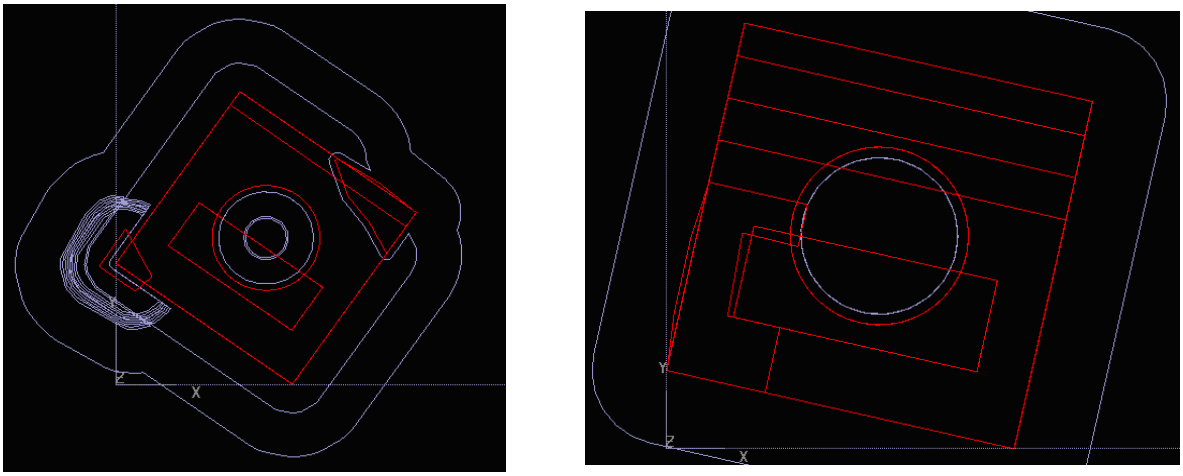

(a) (b)

Figure 2.1: (a) Catalyst EX pre-print view, in which two asymmetric features have appeared at the corners. These features are not present in the STL files prior to their being opened in the Catalyst software. (b) Here again an anomalous 'C'-shaped defect appears on the underside of the particle, in the bottom left corner.

General particle shapes corresponding to those seen in Figures 2.2 and 2.3 were drawn up in Solidworks with varying front taper angles, and different heights. Changing the angle of the taper had a relatively intuitive effect on particle locomotion; the steeper the forward tilt, the greater the forward velocity. Less obvious was the effect increasing the thickness would have on activity. Some speculative reasons for this are discussed in the next section. The vertical symmetry and 'upper foot' (Fig 2.3) were meant to test whether or not impacting the ceiling in the same manner as that of the floor, and effectively doubling the interaction frequency could increase particle

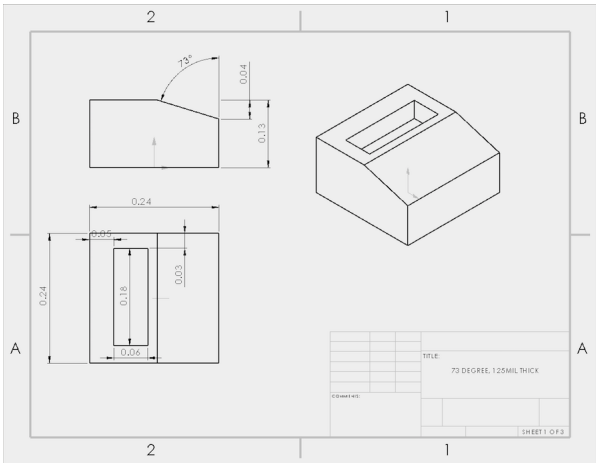

Figure 2.2: Particle with single beveled edge seen from the underside. This design would ultimately become the most successful. Most of the data taken was with particles of this general design, with varying height and incline.

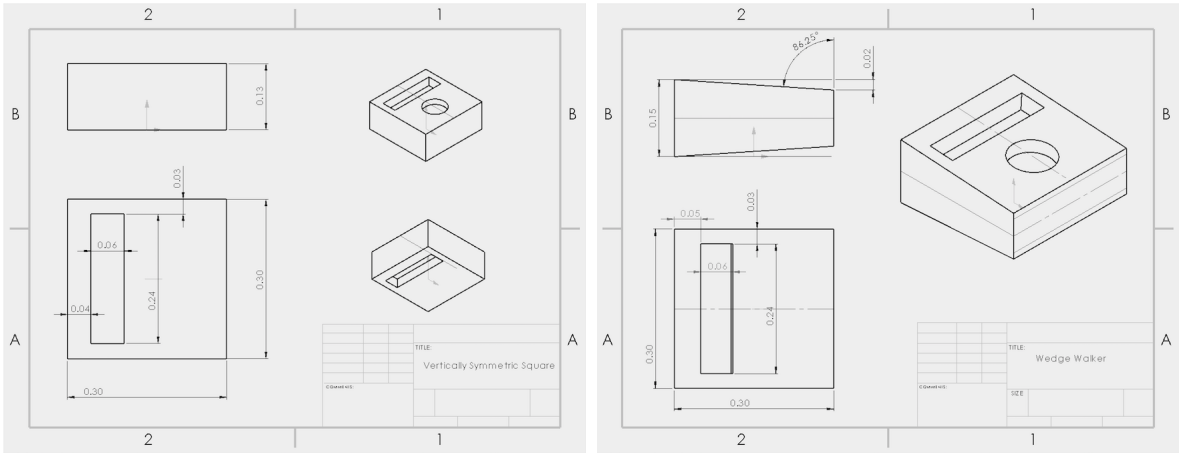

Figure 2.3: Vertically Symmetric Square (left) and Wedge Walker (right). Two alternative particle designs, each with two feet, one on top, the other on the bottom facet. Wedge Walker has an additional bevel on its upper facet. The idea in each case was to try and increase the activity by effectively doubling the frequency of interaction that drives the particle.

persistence length. However this alteration seemed to reduce activity if anything. It was found that locating the trough farther from the center of the particle increased the level of activity. Increasing trough length had the effect of decreasing rotational noise. This was limited by a minimum necessary wall thickness between the trough and the exterior of the particle for reasons of structural stability.

2.2 Particle Locomotion

Of crucial importance is the thickness of the particle, or more accurately the size of the gap between the top of the particle and the lid of the chamber. It is possible that reducing this distance has the effect of tamping down on unwanted rotational motion. The motion of the particles appears far more chaotic when they have a greater degree of out-of-plane rotation available to them. Asymmetrically impacting the plate or ceiling with a single edge or corner results in a significant degree of torque, and thus rotation. Increasing the angular noise results in a much shorter rotational diffusion time, and thus a decreased persistence length. It is possible that reducing their available headroom allows for less angular play and yields an even contact between the bottom face of the particles and the plate more of the time. Increased angular freedom might also help explain the lack of persistent motion in the vertically symmetric particles which have an extra pivot point, and less printed material on their topsides. It has also been suggested that decreasing the headroom and thus vertical travel distance, could result in some type of locked motion of the type observed by Yamada *et al.*[10]

The difference in the motion executed by the particles with a reduced gap between them and the plate is quite stark[3]. Thinner or vertically symmetric particles had persistence lengths of less than one particle size and their motion appeared brownian. Adjusting the driving amplitude and frequency we were able to vary persistence length in a consistent way, but the effect was still mild. However by varying the allowed space between particle and lid, the persistence length grows to nearly three times the particle size. They appear to be the definition of active particles with a very persistent forward motion. Though it was nearly impossible to continuously vary the particle thickness, now that a working design has been found it can be fixed. With

[3] two comparison videos can be found here: https://drive.google.com/open?id=0B2lPtxuQlxg6Q2RWRXJwa3RYZW8

this realization we need now tune only a single parameter: the frequency. This we are able to do continuously.

Lower vibration frequencies result in increased activity (see tables in section 2.3). Intuitively one would expect that in the ultra-low frequency limit activity should disappear. As yet we have not found the low frequency limit, where particle activity begins to decline. Exploring this region of parameter space is complicated by the interplay between driving amplitude and frequency, and the potential for a mechanical over-travel that could damage the system. The shaker is driven with a programmed amount of force, which is sinusoidally varying. The degree to which the driving signal voltage is amplified, and the conversion from volts to driving force by the electromagnetic shaker have not been fully worked out. The mechanical response of the shaker to a range of frequencies and driving voltages has been measured directly however (Fig 2.4).

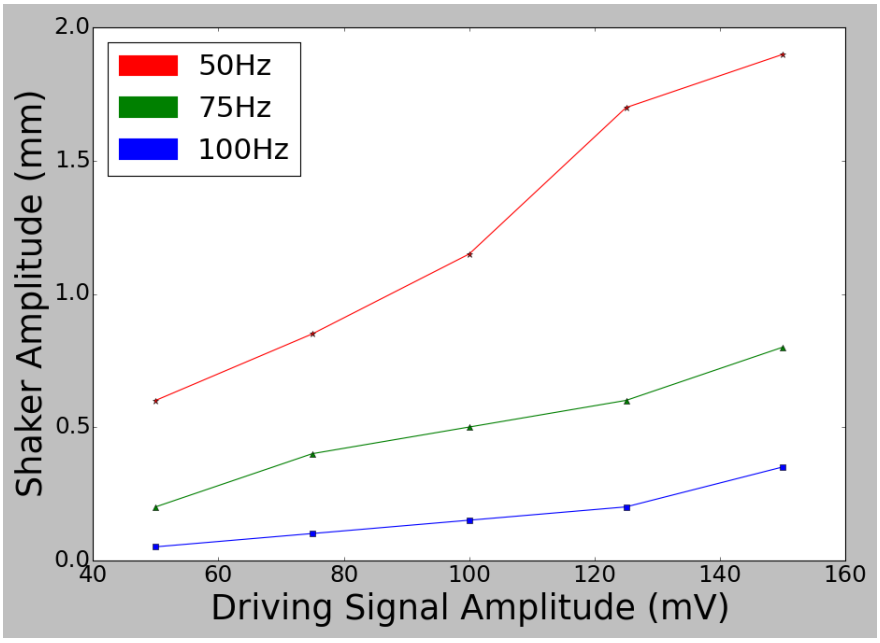

Figure 2.4: Physical amplitude of the shaker cell as a function of driving signal amplitude and frequency.

2.3 Statistics of Particle Motion

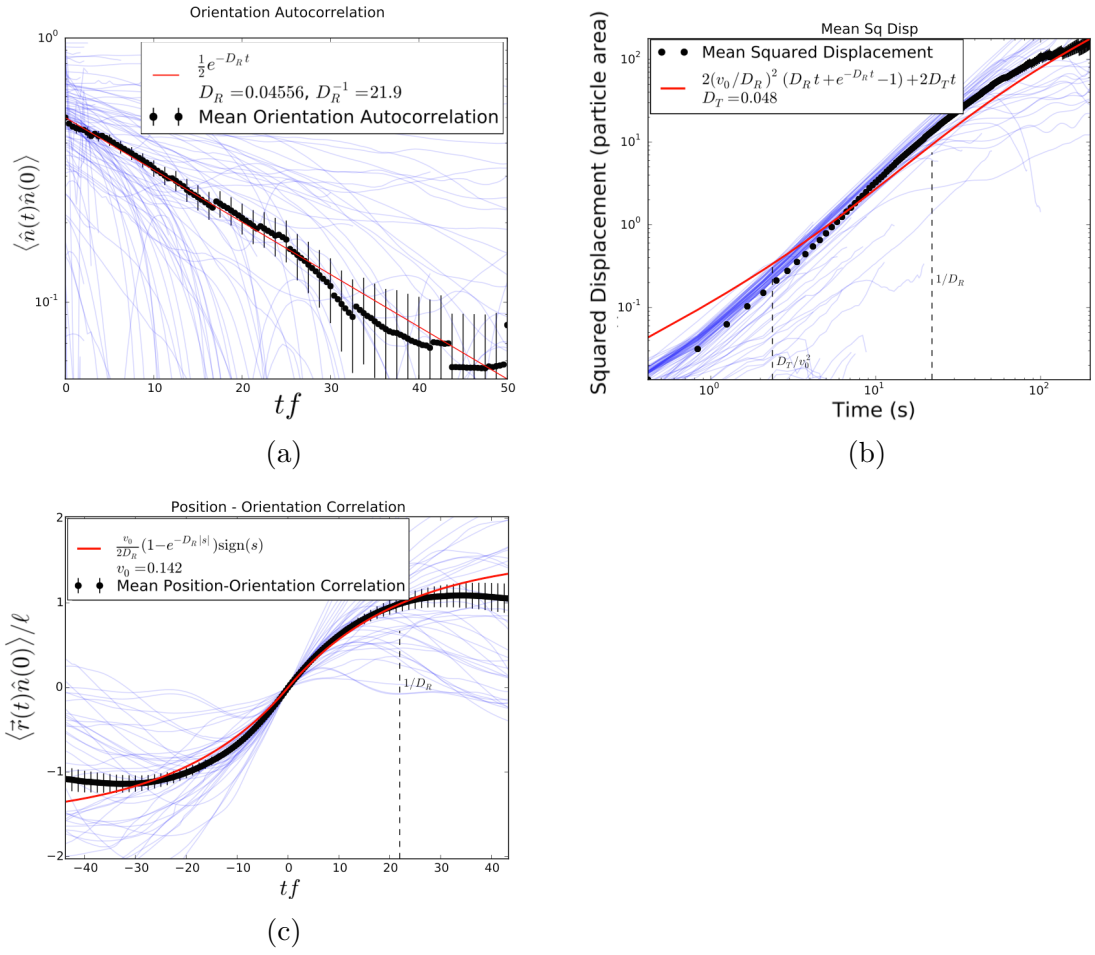

Figure 2.5: Plotted here are the (a) $< \vec{n}\vec{n} >$, (b) $< \vec{r}\vec{r} >$, and (c) $< \vec{r}\vec{n} >$ for a single set of operating parameters. A 125mil thick particle with a relatively steep bevel, shaken at $50Hz$ with a driving signal amplitude of $100mV$. The dashed lines in plots (b) and (c) indicate the rotational or translational diffusion times.

Early experiments carried out by Sarah Schlossberg and Lee Walsh determined that data could be taken on sets of up to 16 particles without the statistics showing any dependence on density. As a result, all of the data gathered on particle locomotion were taken in this dilute limit. Plots of the type shown in Fig. 2.5 (along with the persistence length $\frac{V_0}{D_R}$) were generated by Lee's tracking software. These were the main means of assessing a particle's activity, and the degree to which it conformed to the predicted model.

The orientation (Fig. 2.5a), driven purely by noise should see an exponential decay in correlation with time. At early times this appears to hold, with the fit growing worse with increasing time. The free parameter in fitting here is D_R. With small numbers of particles the cessation of any given particle track can strongly affect the average. This is part of the reason for the discontinuities in the plot.

The case of position-orientation cross correlation is quite similar (Fig. 2.5c), a certain qualitative likeness, but poor fitting. This measures the degree to which a particle's present position depends on its earlier orientation. One expects a strong initial correlation that gradually tapers as dissipative forces sap the particle of its initial momentum, and as the orientation drifts due to noise. D_R has already been fixed in fitting $< \vec{n}\vec{n} >$. This constraint is one reason for the difficulty in fitting. Here $V_)$ is the free parameter.

The mean squared displacement (Fig. 2.5b) is displayed on a log-log plot. A slope of $\frac{1}{2}$ indicates diffusive motion, and 1 ballistic motion. The particles show the appropriate qualitative behavior in that it is something like diffusive at short times, ballistic within an intermediate time-scale, and then bends back toward diffusive behavior at long time scales. From this graph D_T is generated while $D_R, and V_0$ from the previous fittings are held fixed. So far the majority of the fits are still unsatisfactory and, taken with the rest of the plots, suggest that some of the assumptions of the model are up for debate. Specifically the assumption of delta correlated noise has begun to be scrutinized more carefully [26]. In examining the videos taken there is little doubt that the particles display a greatly increased activity, but the values of our fit parameters should be regarded with some suspicion.

Fitting has been complicated by the lack of a satisfying means of weighting the data points, and doing a simultaneous cross-fit in determining the parameters V_0, D_R, and D_T. Currently $< \vec{n}\vec{n} >$ is fit first with only a single fit parameter, D_R. D_R is then fixed, and $< \vec{r}\vec{n} >$ is fit with V_0 as the only free parameter. The MSD is finally

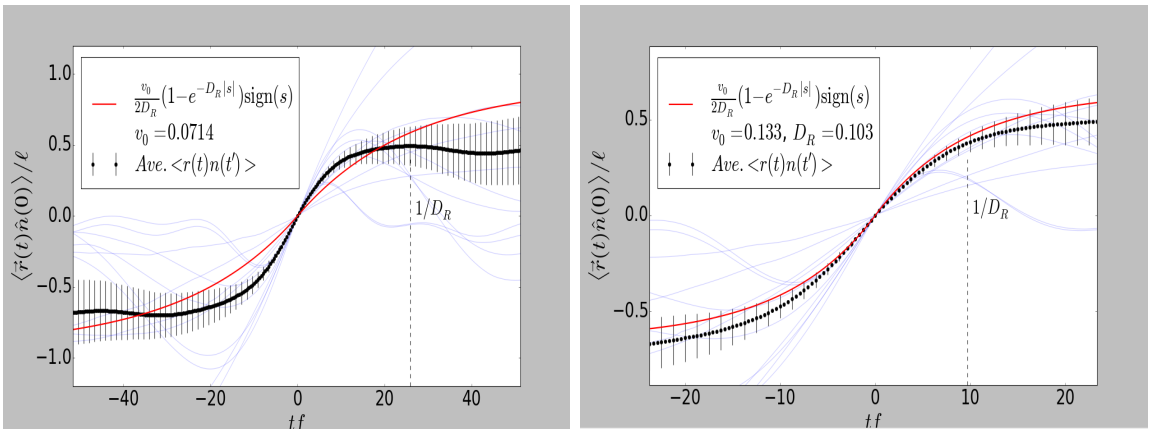

Figure 2.6: The difference between fitting with one (left) and two (right) free parameters in $< \vec{n}\vec{n} >$.

fit with only D_T as a free parameter. Each fit may be done independently leaving all three parameters free, but this usually generates conflicting values for V_0 and D_R (Figure 2.6). Each datapoint is weighted by the size of its standard error. The fact that there are fewer long tracks necessarily skews some of the weighting at longer times. As time goes on there are fewer continuous tracks to average, and a larger dispersion of the data about that average.

From these plots tables of different particle properties, under different operating conditions, was assembled (Fig 2.7). High forcing-amplitude coupled with a low driving frequency result in increased activity. There also appears to be a marked decrease in the persistence length at driving frequencies above $50Hz$.

Figure 2.7. Tables of Active Particle Statistical Properties. Various particle types are listed, labeled by their working title, angle (if any), version number, thickness, and gap between particle and ceiling. For each particle type the persistence length ($\frac{V_0}{D_R}$) is given for several values of Γ. The tables are listed according to the frequency at which the shaker was driven. (below: 50hz)

Particle, (Version), Thickness (in mil), Headroom (in mil)	Acceleration (in g)	v0/DR
Wedge 86.25° (1.2), 150, 62	3.62	0.309
	5.39	0.488
	7.32	0.588
Vertically Symmetric Square (1.1), 150, 62	3.62	0.114
	5.39	0.15
	7.32	0.159
71° (1.0) 120, 100	3.62	0.053
	5.39	0.251
	7.32	0.44
69° (1.0) 120, 100	7.32	0.691
73° (1.0) 120, 100	3.62	0.061
	5.39	0.294
	7.32	0.564
	9.05	0.534
	10.98	0.551
73° (1.3) 125, 80	5.39	0.594
	7.32	0.72
	9.05	0.756
	10.98	0.847
69°(1.0), 125, 4	7.32	3.056
	10.98	1.934
	11.87	2.254
73°(1.0), 125, 4	7.32	2.178
	10.98	2.16
	11.87	1.868

Particle, (Version), Thickness (in mil), Headroom (in mil)	Acceleration (in g)	v0/DR
73° (1.0) 120, 100	3.31	0.32
	4.93	0.074
	6.47	0.047
	8.28	0.222
	9.82	0.364
73° (1.3) 125, 80	3.31	0.177
	4.93	0.03
	6.47	0.094
	8.28	0.215
	9.82	0.322

Figure 2.8: Particles at 75hz (above) and 100hz (below)

Particle, (Version), Thickness (in mil), Headroom (in mil)	Acceleration (in g)	v0/DR
73° (1.0) 120, 100	2.92	0.169
	4.31	0.113
	5.54	0.061
	6.93	0.133
	8.67	0.046

As mentioned, the angle of the bevel on the particle's leading edge has a somewhat obvious effect (the steeper the bevel, the higher the particle's intrinsic velocity). Vertical symmetry of interaction (Fig. 2.3) did not appear to aid in any persistent motion.Those particles with a design like that of Fig 2.2, a height of 125mil, with .12 mm headroom, and a single tapered edge of 69 degrees have the highest persistence length measured so far. This design which prevents any particle overlap has effectively solved the two major problems plaguing the original experiments on crystal melting. Figures 2.9 and 2.10 below summarize some of the above data.

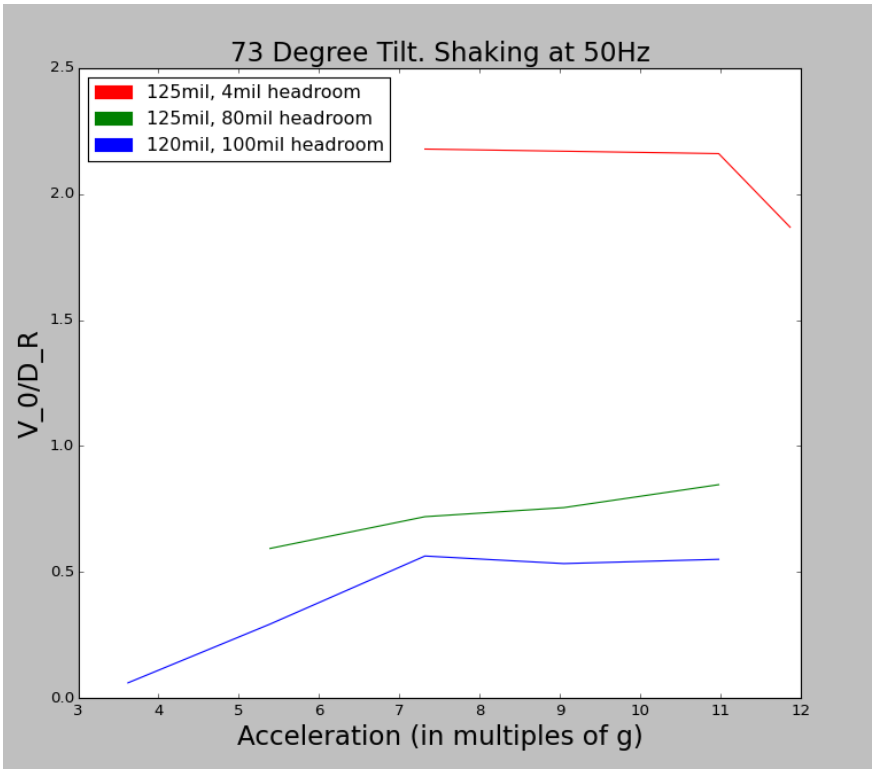

Figure 2.9: The persistence length for the same particle design driven at 50hz, for various amplitudes and spacings.

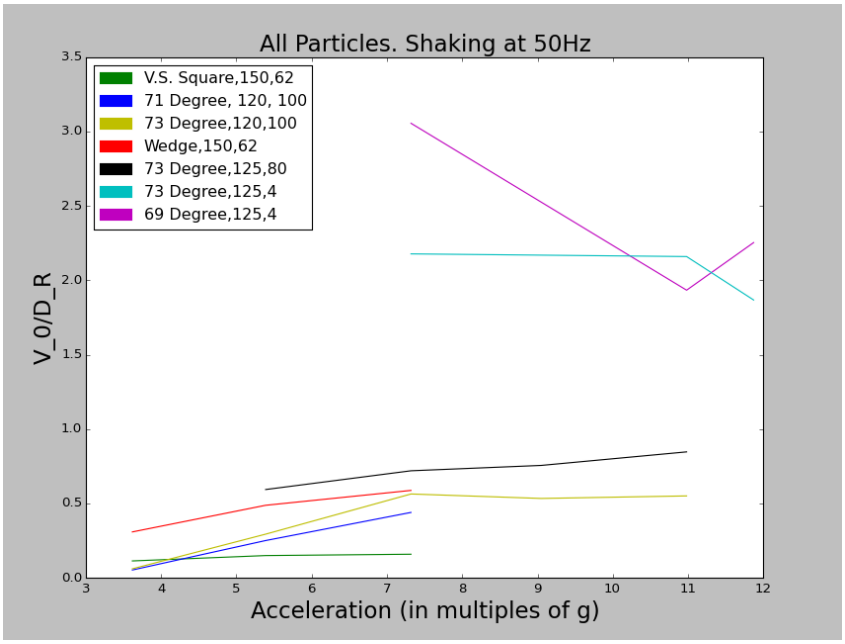

Figure 2.10: The persistence length of each particle design, driven at 50, for various amplitude spacings

2.4 Start-Up

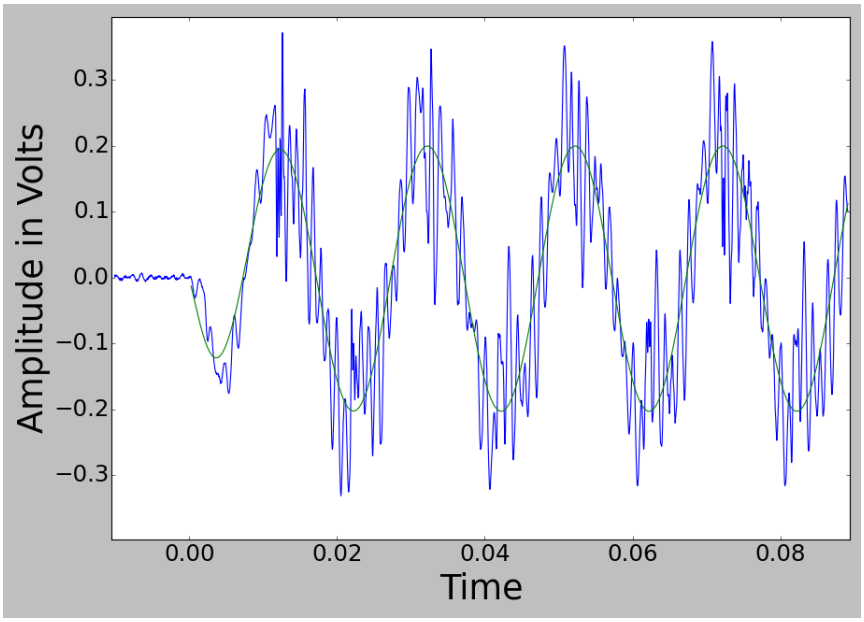

Figure 2.11: Plotted here is an average of numerous accelerometer readings taken at 50Hz. The averaged signal is fit to a function: $A\left(1-e^{-t/\tau}\right)\sin\left(2\pi\, ft+\phi\right)+C$, which is also plotted here. The shaker smoothly approaches a sinusoidal oscillation in under one period. The high frequency noise present in the above image is remarkably consistent across runs. This prompted an examination of of possible resonant modes in the system.

The possibility of a sharp initial transient in the driving signal resulting in a mechanical over-travel or exceeding the maximum force limit of the shaker was concerning. To ensure a certain smoothness in bringing the system up to its operating conditions, the gain of the driving signal was originally increased manually, and rather slowly when compared to the relevant timescales of the experiment. This complicated any investigation of crystal melting where the original goal was to take a lattice from zero effective temperature to well above its melting point in a very short timespan. Preliminary data on particles in a lattice had shown an anomalously high rate of increase in the MSD of particles at early times. It had been suggested that some aspect of the shaker start-up, the slow approach to operating conditions, and the possibility of passing through an unexpected mechanical resonance may have played a part

in generating this increase. Part of my work involved checking the startup driving signal and response in order to get a sense of the time it takes to achieve operating conditions and in order to ensure that the system didn't exceed any mechanical limits.

Figure 2.11 demonstrates rather clearly that the system is capable of approaching operating conditions relatively smoothly, achieving the desired amplitude and frequency in less than one oscillation cycle[4]. The high frequency noise present in the accelerometer data was surprisingly consistent across runs, and along with the spike in particle MSD at early times prompted a look into any resonant modes present in the system.

[4]The fit coefficients are $A = -2.01e-01(V)$, $\tau = 47.3(s^{-1})$, $f = 4.99e+01(s^{-1})$, $\phi = 8.73643591e-01$, $C = -1.56e-03(V)$.

2.5 Resonance

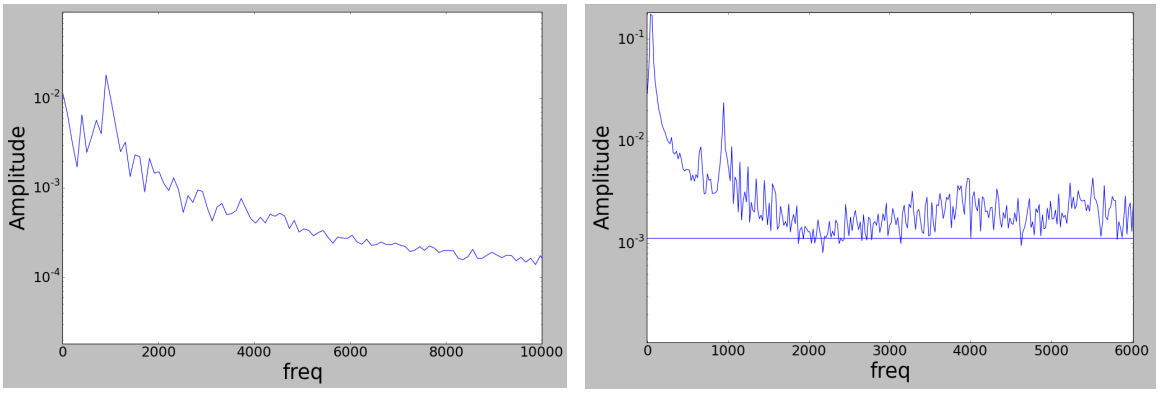

(a) (b)

Figure 2.12: Semi-log plots of the power spectrum of the shaker. Averaged over numerous runs. Image (a) shows the typical response of the bare plate and column after receiving a brief impulse. Image (b) is the result of driving the plate at 50Hz, with particles and chamber included.

Spectral data was taken with the triaxial accelerometer, and measured the response of the system to a number of different impulses. The accelerometer was attached to the cell of the shaker. Its amplified signal was measured with a Tektronix TDS 1012B digital storage oscilloscope. The shaker was excited through mechanical impulse (tapping or knocking). The normalized discrete fourier transform of the response signal was generated in order to look for any resonant mechanical modes in the system. Data was also taken while driving the system at 50Hz with a signal amplitude of 100mV, in the presence of a typical amount of particles. The averaged data from many runs is plotted below on a semi-log plot. Comparing the two plots it can be seen that the presence of particles and external forcing contribute no new resonant modes of interest, and that the driving frequency is an order of magnitude larger than any other mode present in the system. There exist no real peaks of interest in the spectrum below 1kHz, which is well above any frequency relevant to our experiments.

It would seem then, that the initial increase in MSD of the particles is less the result of an uneven start-up, or an unintended resonance and more likely to do with the particles themselves, the nature of the phase transition, or the shape entropy.

CHAPTER 3

CONCLUSIONS AND FUTURE WORK

The goal at the outset was to characterize the effects of activity on the melting of a 2D non-cohesive crystal. This is done by taking a condensed lattice of active particles and instantaneously bringing it from 'zero' temperature to above its melting point by vibrating the plate on which it rests. One could then examine the evolution and loss of the system's orientational and translational order as melting occurs. Related work describing the phase diagram, spatial structure, and order parameter behavior for *in*-active squares has been carried out [20-23] and provides an important set of comparison cases.

Preliminary work with active squares had been carried out by Michael Mueller and Lee Walsh, who looked into the changes in density, as well as rotational order as a function of time and particle location within a finite crystal. The experiment and subsequent analysis were never fully completed as they suffered from a number of issues at that time. Two of the biggest ones were the already mentioned issues of overlap (less than square particles) and the fact that the particles under study had such low persistence lengths.

Both issues have effectively been solved, and a working particle design has been found. A third issue raised by the preliminary work has also been resolved, that of the shaker start-up. Which features of the solid-liquid transition were dependent on the particles, and which were a function of the slow start-up time was unclear. That the system can be triggered with a single button, smoothly reach its programmed amplitude in less that one oscillation period without damaging the system, and that

the initial burst of activity is not due to any feature of shaker startup, have all now been shown. The system lacks any significant resonant peaks at frequencies lower than $1kHz$, putting the first significant resonance well above the cutoff for a complete high-frequency loss of activity.

Given recent improvements in particle design, and with a better understanding of the mechanical properties of the system the remaining barriers to examining the effects of activity on crystal melting appear to be largely analytical or model related. For instance, the issue of appropriately defining per-particle density in a finite system (where particles on the edge have effectively zero density since they are unbounded on one side) or the fact that assumptions of delta correlated noise may not hold up and certain model parameters may change as a result. Future work should consider gathering statistics at intervals in phase with the shakes of the system, which might improve fitting through fewer dropped tracks. It would also be helpful to obtain a clear relation between driving signal voltage and the applied force of the electromagnet so as to explore the full range of allowed system parameters without causing damage. Having found what appears to be a truly active particle, and a means of continuously varying the activity the stage is now set to continue examining the effect of activity on melting in granular media.

REFERENCES

1. S. Ramaswamy, Annual Review of Condensed Matter Physics, 1, pp. 323-345, (2010)
2. M. C. Marchetti, J. F. Joanny, S. Ramaswamy, T. B. Liverpool, J. Prost, Madan Rao, and R. Aditi Simha Rev. Mod. Phys. 85, 1143, (2013)
3. A. Cavagna, and I. Giardina, Annual Review of Condensed Matter Physics, 5, pp. 183-207, (2014)
4. S. Gueron, S.A. Levin, and D.I. Rubenstein, J. Theor. Biol., 182, 85-98, (1996)
5. J. Toner, Y. Tu, and S. Ramaswamy, Annals of Physics 318 (1), pp. 170-244, (2005)
6. J. Toner, and Y. Tu Phys. Rev. E 58, 4828, (1998)
7. J. Toner and Y. Tu Phys. Rev. Lett. 75, 4326, (1995)
8. S. Ramaswamy, R. Aditi Simha and J. Toner, Europhys. Lett., 62 (2), pp. 196-202, (2003)
9. V. Narayan, S. Ramaswamy, N. Menon, Science, 317 (5834), pp. 105-108, (2007)
10. D.Yamada, T. Hondou, and M. Sano Phys. Rev. E 67, 40301,(R) (2003)
11. B. M. Mognetti, A. Saric, S. Angioletti-Uberti, A. Cacciuto, C. Valeriani, and D. Frenkel Phys. Rev. Lett. 111, 245702, (2013)
12. J. Palacci, S. Sacanna, A. P. Steinberg, D. J. Pine, P.M. Chaikin, Science, 339 (6122) pp. 936-940, (2013)
13. S. Thutupalli, R. Seemann and S. Herminghaus, New Journal of Physics, 13, (2011)
14. J. Deseigne, O. Dauchot, and H. Chat, Phys. Rev. Lett., 105, 098001, (2010)
15. D. Helbing, Rev. Mod. Phys., 73, 1067, (2001)
16. N. Kumar, H. Soni, S. Ramaswamy and A.K. Sood, Nature Communications, 5, (4688), (2014)
17. T. Vicsek, A. Czirk, E. Ben-Jacob, I. Cohen, and O.Shochet Phys. Rev. Lett. 75 (6), 1226, (1995)
18. T. Vicsek, A. Zafeiris, Physics Reports, 517, pp. 71-140, (2012)
19. T. Vicsek, A. Czirk, E. Ben-Jacob, I. Cohen, and O. Shochet, Phys. Rev. Lett., 75 (23), (1995)
20. K. Zhao, R. Bruinsma, and T.G. Mason, PNAS, 108 (7), pp. 2684-2687, (2010)
21. Avendano, and F.A. Escobedo, Soft Matter, 8, pp. 4675-4681, (2012)
22. Lee Walsh, Dissertation Prospectus, University of Massachusetts, (2014)
23. Lee Walsh, and N. Menon, arXiv:1510.00656v1, [cond-mat.soft]

24. V. Balakrishnan, Elements of Nonequilibrium Statistical Mechanics (CRC Press, 2008).
25. R. Zwanzig, Nonequilibrium Statistical Mechanics (Oxford University Press, 2001), 1st edition.
26. Private communication, unpublishednotesofAparnaBaskaran (Brandeis University).